Supporting Information

Construction of an Autonomously Concatenated Hybridization Chain Reaction for Signal Amplification and Intracellular Imaging

Jie Wei,[a] *Xue Gong,*[a] *Qing Wang*,[a] *Min Pan*,[a] *Xiaoqing Liu,*[a] *Jing Liu,*[b] *Fan Xia,*[c] *Fuan Wang*[*,a]

[a] Key Laboratory of Analytical Chemistry for Biology and Medicine (Ministry of Education), College of Chemistry and Molecular Sciences, Wuhan University, Wuhan 430072, P. R. China

[b] Department of Gastroenterology, Zhongnan Hospital of Wuhan University, Hubei Clinical Center & Key Lab of Intestinal & Colorectal Diseases, Wuhan 430072, P. R. China

[c] Department of Urology, Union Hospital, Tongji Medical College, Hubei Key Laboratory of Bioinorganic Chemistry & Materia Medica, School of Chemistry and Chemical Engineering and Department of Epidemiology and Biostatistics, School of Public Health, Tongji Medical College, Huazhong University of Science and Technology (HUST), Wuhan 430074, P. R. China

[*] To whom correspondence should be addressed. E-mail: fuanwang@whu.edu.cn.

Table of Contents

Table S1. The DNA sequences used to construct the amplified sensing platform

No.	Sequence (5'→3')
H_1	5'-GGA ATT CGG AGC TAG GTA GGT AGA GTA ATG CCG TCT ACC TAC CTA GCT CCG-3'
H_2	5'-GCT TCA TCT TCA TCT CCG TCT ACC TAC CTA GCT CCG AAT TCC CGG AGC TAG GTA GGT AGA CGG CAT TAC ACA CTC-3'
H_{1A}	5'-GCT TCA TCT TCA TCT CCG GGA ATT CGG AGC TAG GTA GGT AGA CAT TAC TCT ACC TAC CTA GCT CCG ACA CTC-3'
H_{2A}	5'-TCT ACC TAC CTA GCT CCG AAT TCC CGG AGC TAG GTA GGT AGA GTA ATG-3'
H_3	5'-GAG TGT CGG AGA TGA AGA TGA AGC CAT CGT GCT TCA TCT TCA TCT CCG-TAMRA-3'
H_4	5'-GCT TCA TCT TCA TCT CCG GTT TTG CGG AGA TGA AGA TGA AGC ACG ATG-3'
H_5	5'-FAM-CAA AAC CGG AGA TGA AGA TGA AGC TTG CCT GCT TCA TCT TCA TCT CCG-3'
H_6	5'-GCT TCA TCT TCA TCT CCG ACA CTC CGG AGA TGA AGA TGA AGC AGG CAA-3'
H_7	5'-ATC AGA CTG ATG TTG AGG TCT ACC TAC CTA GCT CCG AAT TCC TCA ACA TCA GTC TGA TAA GCT A-3'
I	5'-TCT ACC TAC CTA GCT CCG AAT TCC-3'
I_A	5'-TCT ACC TAC CTA GCT CCG AA**A** TCC-3'
I_B	5'-TCT ACC TAC CTA GC**A** CCG AA**A** TCC-3'
I_C	5'-TCT ACC **A**AC CTA GC**A** CCG AA**A** TCC-3'
T_I	5'-GCT TCA TCT TCA TCT CCG TCT ACC TAC CTA TTT TTT-3'
T_{II}	5'-TTT TTT GGT ATA CGG CAT TAC ACA CTC-3'
T_{III}	5'-AAA AAA TAG GTA GGT AGA GTA ATG CCG TAT ACC AAA AAA-3'
miR-21	5'-UAG CUU AUC AGA CUG AUG UUG A-3'
let-7a	5'-UGA GGU AGU AGG UUG UAU AGU U-3'
son DNA	5'-ACU CCC AGA UGU UAG CAA C-3'
β-actin mRNA	5'-GCA AGC CAU GUA CGU UGC UAU CCA GGC UGU GCU AUC CCU GU-3'

Table S2. The DNA sequences for C-HCR imaging of living cells

No.	Sequence (5'→3')
H_1*	5'-G*G*A* ATT CGG AGC TAG GTA GGT AGA GTA ATG CCG TCT ACC TAC CTA GCT *C*C*G-3'
H_2*	5'-G*C*T* TCA TCT TCA TCT CCG TCT ACC TAC CTA GCT CCG AAT TCC CGG AGC TAG GTA GGT AGA CGG CAT TAC ACA *C*T*C-3'
H_3*	5'-G*A*G* TGT CGG AGA TGA AGA TGA AGC CAT CGT GCT TCA TCT TCA TCT *C*C*G-TAMRA-3'
H_4*	5'-G*C*T* TCA TCT TCA TCT CCG GTT TTG CGG AGA TGA AGA TGA AGC ACG *A*T*G-3'
H_5*	5'-FAM-C*A*A* AAC CGG AGA TGA AGA TGA AGC TTG CCT GCT TCA TCT TCA TCT *C*C*G-3'
H_6*	5'-G*C*T* TCA TCT TCA TCT CCG ACA CTC CGG AGA TGA AGA TGA AGC AGG *C*A*A-3'
H_7*	5'-A*T*C* AGA CTG ATG TTG AGG TCT ACC TAC CTA GCT CCG AAT TCC TCA ACA TCA GTC TGA TAA G *C*T*A-3'
miR-21 inhibitor	5’-mU*mC*mA* mAmCmA mUmCmA mGmUmC mUmGmA mUmAmA mG*mC*mU *mA-3’

* = Phosphorothioate Bonds

mN = 2’-*O*-Me RNA base

Validation of the FRET between FAM and TAMRA fluorophores

The FAM/TAMRA fluorophore was applied as a moderate FRET pair to study the C-HCR strategy. As shown in Figure S1, the absorption spectrum of TAMRA fluorophore acceptor has a sufficient spectral overlap with the emission spectrum of FAM fluorophore donor, validating the FRET process can proceed from FAM to TAMRA. This provides the basic readout mechanism for the present C-HCR scheme in signal amplification and intracellular imaging applications.

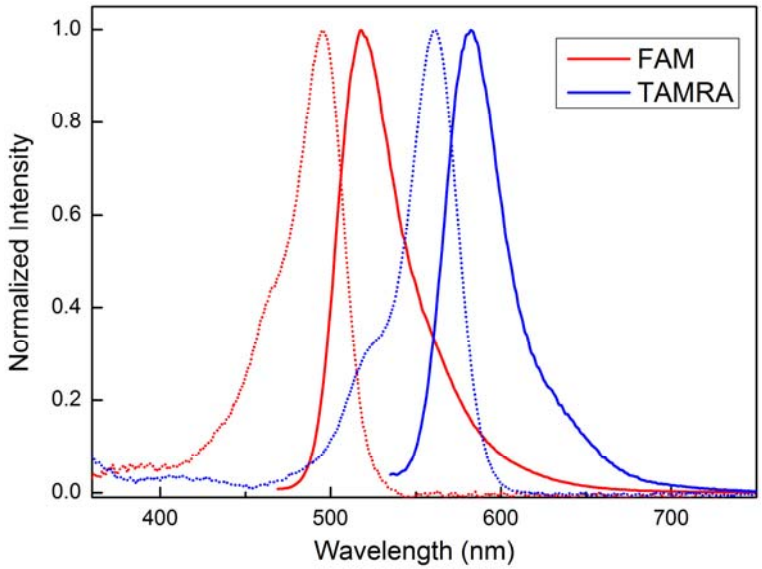

Figure S1. The absorption and emission spectra of the fluorophore donor (FAM) and acceptor (TAMRA). A sufficient spectral overlap between the absorbance of TAMRA and the emission of FAM enables an efficient FRET transduction from FAM fluorophore to TAMRA fluorophore.

Schematic illustration of the downstream HCR-2 system

As shown in Figure S2(A), a **T**-analog structure ($\mathbf{T_I/T_{II}/T_{III}}$) containing domain e-d was utilized to activate the downstream HCR-2 circuit, consisting of four DNA hairpins $\mathbf{H_3}$, $\mathbf{H_4}$, $\mathbf{H_5}$ and $\mathbf{H_6}$. The **T**-analog structure ($\mathbf{T_I/T_{II}/T_{III}}$) can open hairpin $\mathbf{H_3}$ by hybridizing with the sequence e*-d* (pink) in hairpin $\mathbf{H_3}$. The opened $\mathbf{H_3}$ releases the sequence f-d (pink) that is complementary to the sequence d*-f* (purple) of hairpin $\mathbf{H_4}$. $\mathbf{H_4}$ then releases the sequence d-g (purple) that hybridizes with the sequence domain g*-d* (pink) of hairpin $\mathbf{H_5}$. The opened $\mathbf{H_5}$ releases the sequence h-d (pink) that is complementary to the sequence domain d*-h* (purple) in hairpin $\mathbf{H_6}$. And $\mathbf{H_6}$ releases the domain d-e (purple) with the same sequence as **T**-analog structure ($\mathbf{T_I/T_{II}/T_{III}}$). Thus the **T**-analog structure ($\mathbf{T_I/T_{II}/T_{III}}$) activates the autonomous cross-opening of hairpins $\mathbf{H_3}$, $\mathbf{H_4}$, $\mathbf{H_5}$ and $\mathbf{H_6}$, leading to the formation of HCR-2-involved dsDNA nanowires. All hybridization events above are based on toehold-mediated strand displacement mechanism. Moreover, $\mathbf{H_3}$ is modified at its 3' termini with a fluorescence acceptor (TAMRA) while $\mathbf{H_5}$ is modified at its 5' termini with a fluorescence donor (FAM). In the absence of **T**-analog structure ($\mathbf{T_I/T_{II}/T_{III}}$), the donor in hairpin $\mathbf{H_5}$ is separated from the acceptor in hairpin $\mathbf{H_3}$, leading to low FRET efficiency. While in the presence of **T**-analog structure ($\mathbf{T_I/T_{II}/T_{III}}$), it motivates HCR-2 and brings two separated fluorophores (FAM and TAMRA) into close proximity, leading to high FRET efficiency. As shown in Figures S2(B) and 2(C), the downstream HCR-2 can be motivated to transduce the readout signal only when the HCR-2 mixture was incubated with **T** (curve b), not the analyte **I**, validating the high specificity of the present HCR-2 system. A dramatically signal cross talk can then be minimized for the subsequent C-HCR (HCR-1/HCR-2) circuit.

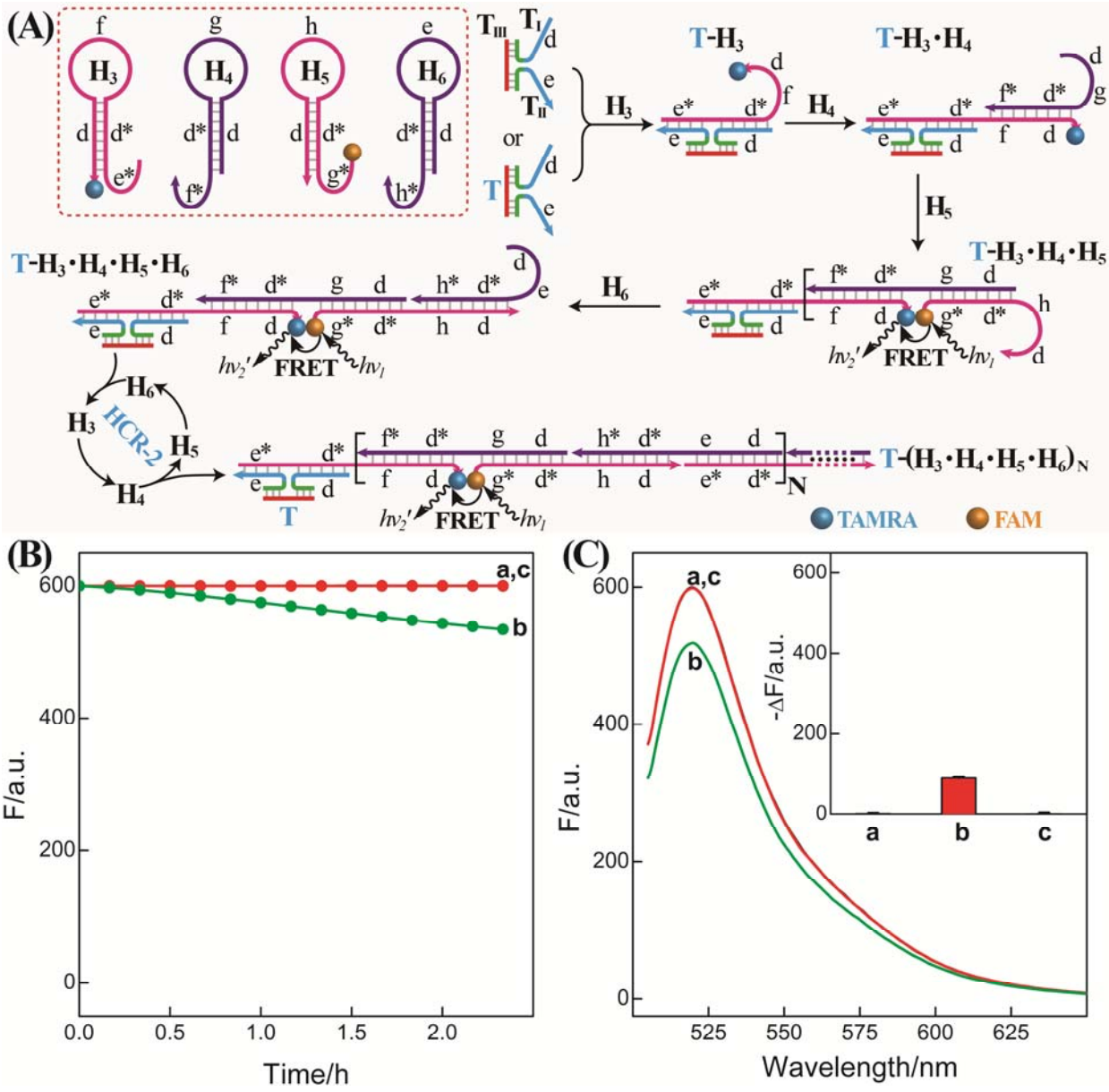

Figure S2. (**A**) The scheme for downstream HCR-2 to transduce the colocalized structure **T**, products of upstream HCR-1, into a fluorescence readout signal. The trigger **T** motivates the multiple sequential cross-opening of $\mathbf{H_3}$, $\mathbf{H_4}$, $\mathbf{H_5}$ and $\mathbf{H_6}$ to produce long dsDNA copolymer nanowires. This brings the donor/acceptor fluorophore (FAM/TAMRA) pairs into close proximity, and leads to a FRET readout signal. (**B**) Time-dependent fluorescence changes (at λ=520 nm) of the HCR-2 system outlined in Figure S2(A) in the presence of no analyte (a), 50 nM **T** (b) and 50 nM **I** (c). (**C**) Fluorescence spectra generated by the downstream HCR-2 circuit shown in Figure S2(A) in the presence of no analyte (a), 50 nM **T** (b) and 50 nM **I** (c) for a fixed time interval of 2 h. Inset: summary of the results of fluorescence spectra at λ=520 nm. F_0 represents the original fluorescence intensity. The system consisting of $\mathbf{H_3}$+$\mathbf{H_4}$+$\mathbf{H_5}$+$\mathbf{H_6}$ mixture (200 nM each) was carried out in reaction buffer (10 mM HEPES, 1 M NaCl, 50 mM $MgCl_2$, pH 7.2). Error bars were derived from n=5 experiments.

Supporting Information

C-HCR-based construction of a frond-like dsDNA copolymer

For the C-HCR system, each $\mathbf{H_1}$-$\mathbf{H_2}$ pair hybridization event of HCR-1 circuit constitute can produce one HCR-2 copolymeric dsDNA nanowire. The **I**-motivated HCR-1 between $\mathbf{H_1}$ and $\mathbf{H_2}$ generates a tandem structure consisting of numerous reconstituted d-e (blue) structure (**T**) that thus provides massive accessible sprouting stages to activate a downstream HCR-2 between $\mathbf{H_3}$, $\mathbf{H_4}$, $\mathbf{H_5}$ and $\mathbf{H_6}$, leading to the construction of a frond-like dsDNA copolymer nanostructure, as schematically shown in Figure S3.

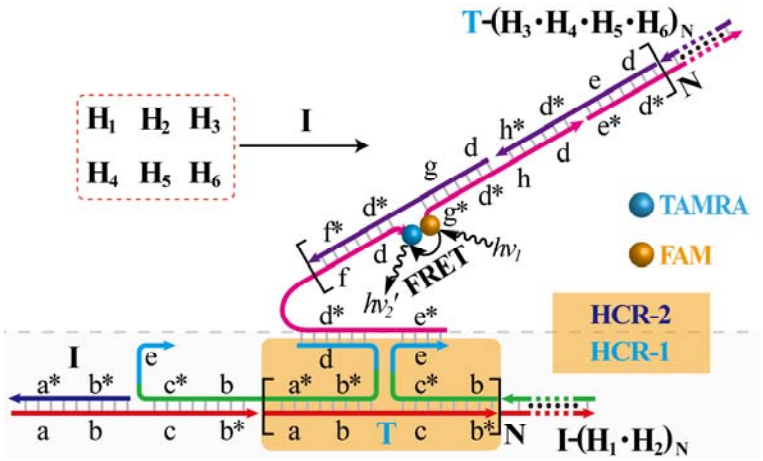

Figure S3. The scheme for the isothermal enzyme-free C-HCR-based construction of a frond-like dsDNA copolymer structure as shown in Figure 1.

Optimization of upstream HCR-1 for the C-HCR-amplified sensing platform

For the effective development of the amplified sensing platform shown in Figure 1, the hairpins $\mathbf{H_1}$ and $\mathbf{H_2}$ should exhibit the following properties: (i) the hairpins ($\mathbf{H_1}$ and $\mathbf{H_2}$) should be retained in fully closed structure prior to their interaction with the initiator to eliminate the false cross-opening and the unwanted background signal. (ii) the hairpins ($\mathbf{H_1}$ and $\mathbf{H_2}$) should exhibit a limited stabilizing energy to enable an effective opening of $\mathbf{H_1}$ by the initiator and the subsequent cross-opening of all the hairpins. Figure S4(A) shows the scheme of the original C-HCR circuit composed of the upstream stem-uncaged HCR-1 system and the downstream HCR-2 system. Figure S4(B) shows the performance of the original concatenated HCR-1/HCR-2 system where the hairpin pair $\mathbf{H_{1A}/H_{2A}}$ composing the upstream HCR-1 has a huge background. That means $\mathbf{H_{1A}}$ can activate HCR-2 system without upstream HCR-1 reconstitution process. However, by caging the fragment d into the stem region of its hairpin, the present hairpin pair $\mathbf{H_1/H_2}$ can dramatically decrease the background signal as shown in Figure S4(C). On the other hand, the initiator triggers an efficient HCR-1 process and the subsequent transducer HCR-2 to yield a significant output fluorescence signal, Figure S4(C). Thus $\mathbf{H_1/H_2}$ hairpin pair was chosen as the optimized components of HCR-1.

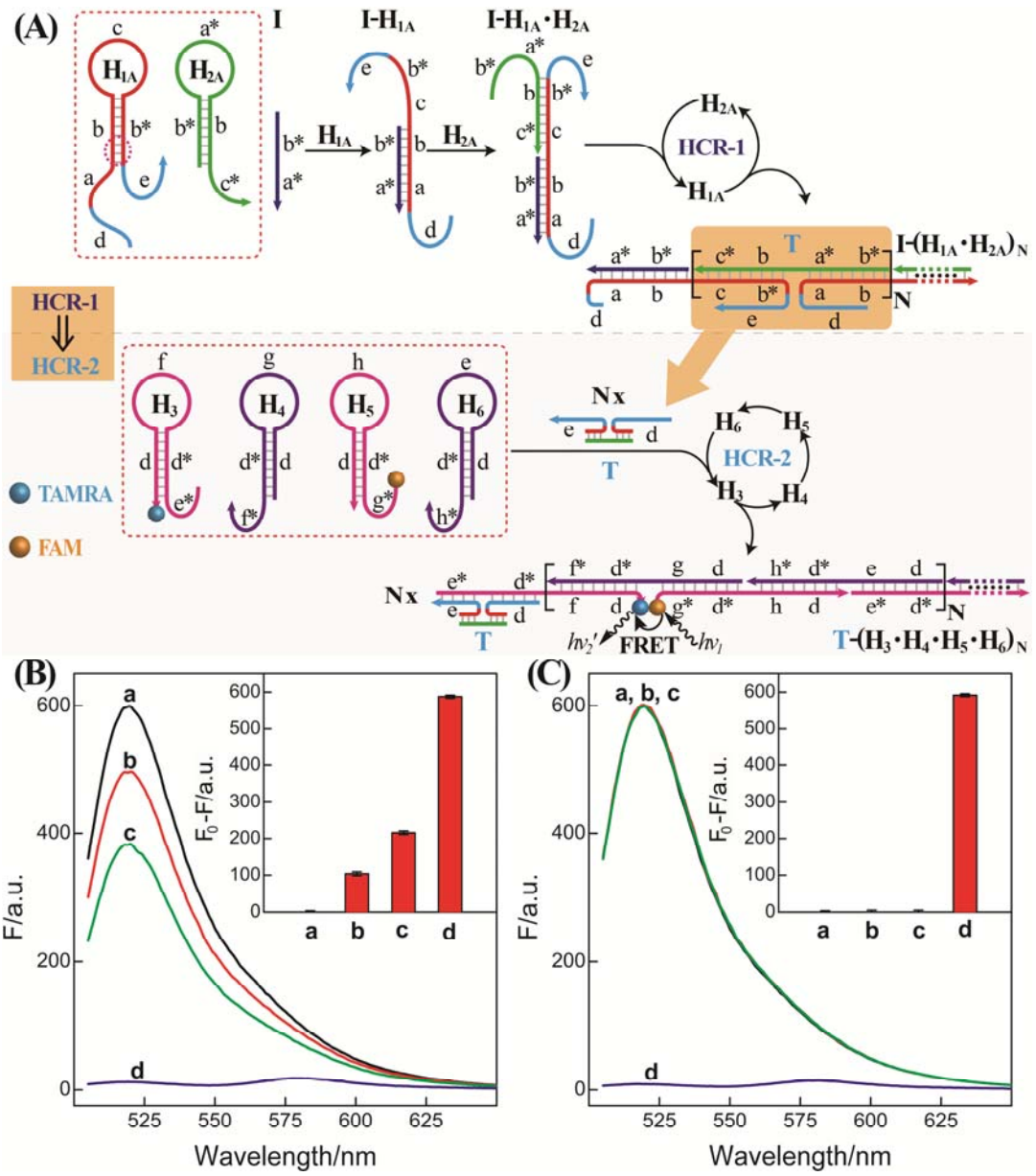

Figure S4. (**A**) The scheme for the original C-HCR circuit composed of the upstream stem-uncaged HCR-1 system and the downstream HCR-2 system. Compared with the optimized C-HCR circuit, segment d herein was not introduced and caged into the stem region of hairpin $\mathbf{H_{1A}}$. The initiator (**I**)-triggered the cross-opening of $\mathbf{H_{1A}}$ and $\mathbf{H_{2A}}$ in the upstream HCR-1 system, yielding dsDNA copolymer consisting of the tandem colocalized structure **T** for transducer HCR-2. (**B**) Fluorescence spectra generated by the original C-HCR system outlined in Figure S4(A) by incubating HCR-2, composed of $\mathbf{H_3}$, $\mathbf{H_4}$, $\mathbf{H_5}$ and $\mathbf{H_6}$ (200 nM each), with different components of the stem-uncaged HCR-1 for a fixed time interval of 2 h: (a) 200 nM $\mathbf{H_{2A}}$, (b) 200 nM $\mathbf{H_{1A}}$, (c) 200 nM $\mathbf{H_{1A}}$ and 200 nM $\mathbf{H_{2A}}$, and (d) 200 nM $\mathbf{H_{1A}}$, 200 nM $\mathbf{H_{2A}}$, and 50 nM **I**. Inset: summary of the results of fluorescence spectra at λ=520 nm. The system was carried out in reaction buffer (10 mM HEPES, 1 M NaCl, 50 mM $MgCl_2$, pH 7.2). (**C**) Fluorescence spectra generated by the optimized C-HCR system shown in Figure 1 by incubating HCR-2, composed of $\mathbf{H_3}$, $\mathbf{H_4}$, $\mathbf{H_5}$ and $\mathbf{H_6}$ (200 nM each), with different components of the stem-caged HCR-1 for a fixed time interval of 2 h: (a) 200 nM $\mathbf{H_1}$, (b) 200 nM $\mathbf{H_2}$, (c) 200 nM $\mathbf{H_1}$ and 200 nM $\mathbf{H_2}$, and (d) 200 nM $\mathbf{H_1}$, 200 nM $\mathbf{H_2}$ and 50 nM **I**. Inset: summary of the results of fluorescence spectra at λ = 520 nm. F_0 represents the original fluorescence intensity. The system was carried out in reaction buffer (10 mM HEPES, 1 M NaCl, 50 mM $MgCl_2$, pH 7.2). Error bars were derived from n=5 experiments.

Supporting Information

Comparison of the amplification efficiency for HCR-2 and C-HCR systems.

It is a characteristic HCR system when the C-HCR mixture was incubated with trigger **T** only since then the downstream HCR-2 is merely activated to transduce the readout signal and the upstream HCR-1 is not involved in the process. As shown in Figure S5, the C-HCR system showed a much higher of fluorescence response over conventional HCR, indicating an enhanced signal amplification efficacy of the C-HCR amplifier (1:N^2) over traditional HCR scheme (1:N).

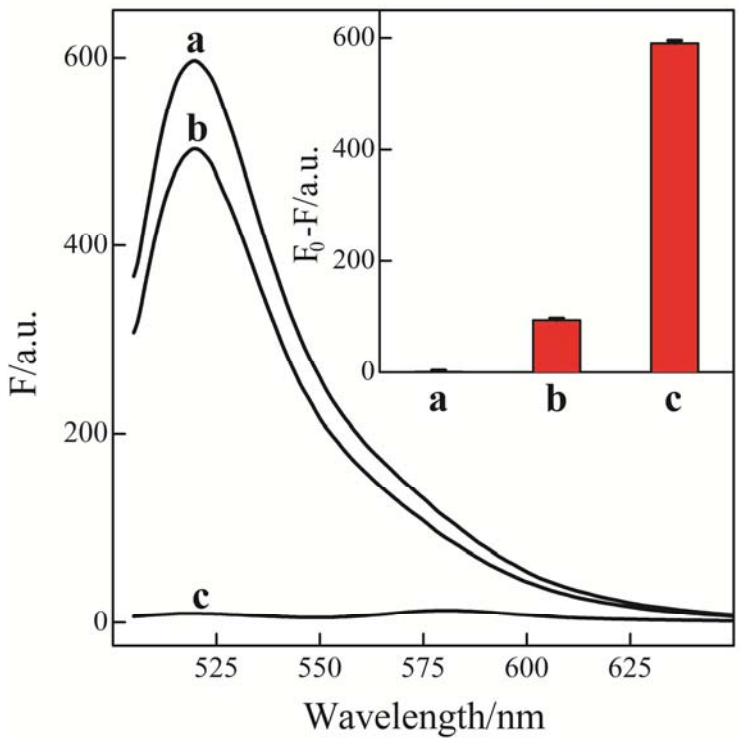

Figure S5. Fluorescence spectra generated by the C-HCR system outlined in Figure 1 in the absence of analyte (a), and upon analyzing 50 nM **T** (b) or **I** (c). Inset: summary of the results of fluorescence spectra at λ=520 nm. F_0 represents the original fluorescence intensity. The system consisting of $\mathbf{H_1}$+$\mathbf{H_2}$+$\mathbf{H_3}$+$\mathbf{H_4}$+$\mathbf{H_5}$+$\mathbf{H_6}$ mixture (200 nM each) was carried out in reaction buffer for a fixed time interval of 2 h. Error bars were derived from n = 5 experiments.

Control experiments by removing one hairpin from the C-HCR mixture

By subtracting $\mathbf{H_1}$ or $\mathbf{H_2}$ from upstream HCR-1, only **T** activates the HCR-2 system, generating a moderate fluorescence change, Figure S6(A) and S6(B), respectively. No fluorescence change can be observed by subtracting $\mathbf{H_4}$ from downstream HCR-2 circuit for the shortage of an important linker between TAMRA- and FAM-labeled $\mathbf{H_3}$ and $\mathbf{H_5}$ hairpins, resulting in no readout transduction even HCR-1 can be activated to generate a copolymeric dsDNA nanowire, Figure S6(C). However, a moderate fluorescence change was observed for **I**-motivated C-HCR system that subtracted $\mathbf{H_6}$ from downstream HCR-2 circuit, while **T**-motivated $\mathbf{H_6}$-subtracted C-HCR system generated a much lower fluorescence change as compared with that of **I**-motivated C-HCR scheme. This can be explicated as follows, for the $\mathbf{H_1}$+$\mathbf{H_2}$+$\mathbf{H_3}$+$\mathbf{H_4}$+$\mathbf{H_5}$ mixture, the absence of $\mathbf{H_6}$ inhibits downstream HCR-2, **T** also generates F/Q hybrid with a ratio corresponding to 1:1, giving rise to a lower FRET signal. However, **I** generates numerous F/Q hybrid based on successive hybridization of upstream HCR-1, giving rise to a moderate FRET signal. This, on the other hand, demonstrate our C-HCR system is based on a concatenated HCR-1/HCR-2 process as shown in Figure 1.

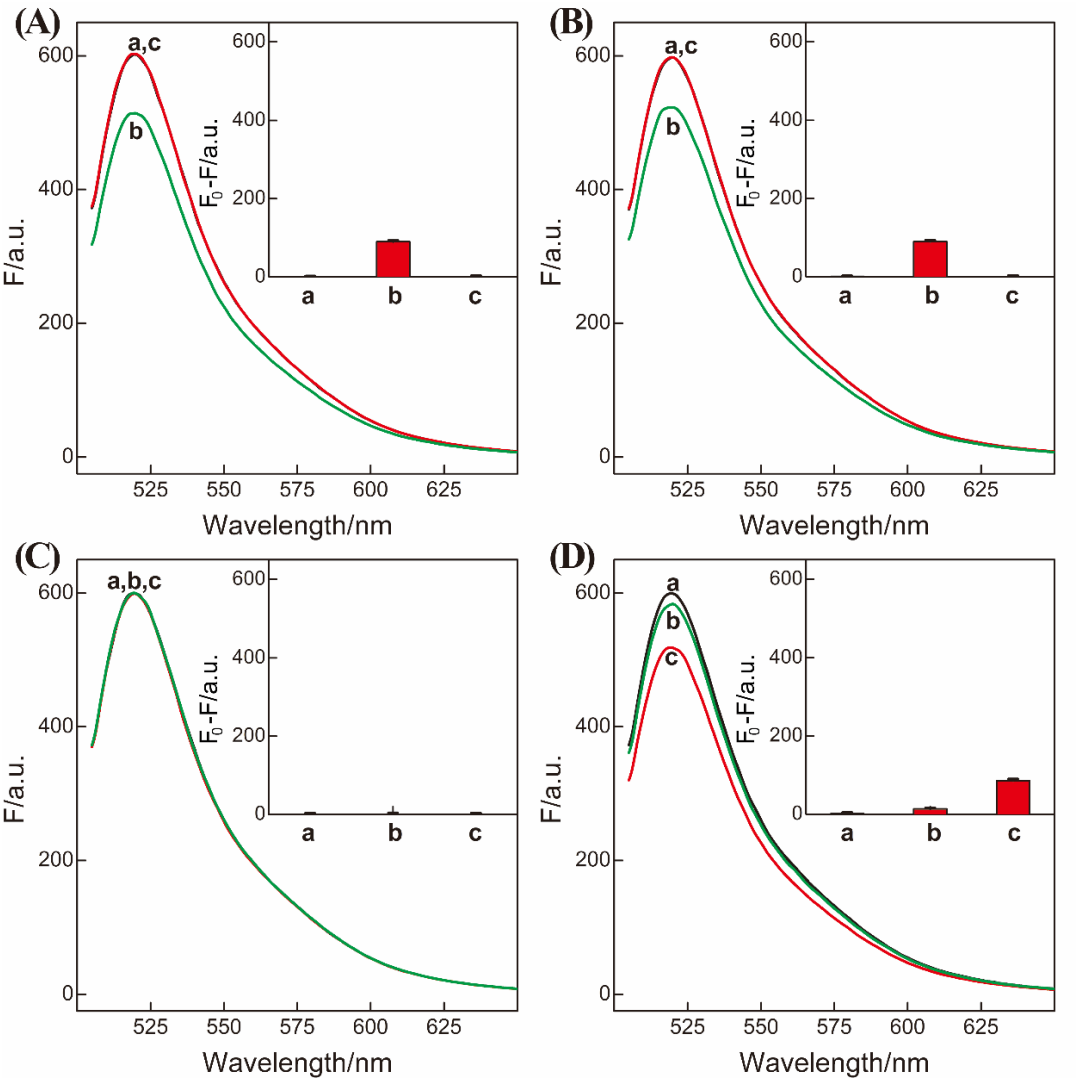

Figure S6. (**A**) Fluorescence spectra generated by the **H_2+H_3+H_4+H_5+H_6** mixture (200 nM each) in the presence of no analyte (a), 50 nM **T** (b), and 50 nM **I** (c) for a fixed time interval of 2 h: Inset: summary of the results of fluorescence spectra at λ=520 nm. (**B**) Fluorescence spectra generated by the **H_1+H_3+H_4+H_5+H_6** mixture (200 nM each) in the presence of no analyte (a), 50 nM **T** (b), and 50 nM **I** (c) for a fixed time interval of 2 h: Inset: summary of the results of fluorescence spectra at λ=520 nm. (**C**) Fluorescence spectra generated by the **H_1+H_2+H_3+H_5+H_6** mixture (200 nM each) in the presence of no analyte (a), 50 nM **T** (b), and 50 nM **I** (c) for a fixed time interval of 2 h: Inset: summary of the results of fluorescence spectra at λ=520 nm. (**D**) Fluorescence spectra generated by the **H_1+H_2+H_3+H_4+H_5** mixture (200 nM each) in the presence of no analyte (a), 50 nM **T** (b), and 50 nM **I** (c) for a fixed time interval of 2 h: Inset: summary of the results of fluorescence spectra at λ=520 nm. F_0 represents the original fluorescence intensity. The system was carried out in reaction buffer (10 mM HEPES, 1 M NaCl, 50 mM $MgCl_2$, pH 7.2). Error bars were derived from n = 5 experiments.

Supporting Information

Comparison of the amplification efficiency for HCR-1 and C-HCR systems.

For comparing the present C-HCR with conventional HCR system, the C-HCR system consisting of **H_1+H_2+H_3+H_4+H_5+H_6** mixture (200 nM each) or the traditional HCR control system (HCR-1 analogues or **H_6**-excluded C-HCR) consisting of **H_1+H_2+H_3+H_4+H_5** mixture (200 nM each) was carried out in reaction buffer (10 mM HEPES, 1 M NaCl, 50 mM $MgCl_2$, pH 7.2) for a fixed time interval of 2 h. The fluorescence intensity changes were acquired at a fixed wavelength of 520 nm. F_0 represents the original fluorescence intensity. Error bars were derived from n=5 experiments. Based on the slope of the linear detection range, C-HCR showed a 25-fold higher of fluorescence response over conventional HCR, indicating an enhanced signal amplification efficacy of the C-HCR amplifier ($1:N^2$) over HCR scheme (1:N).

Supporting Information

Kinetics characterization of the target with different base mutations

To evaluate specificity of the present C-HCR system for DNA detection shown in Figure 1, the sequences of the one-, two-, and three-base mutations $\mathbf{I_A}$, $\mathbf{I_B}$, and $\mathbf{I_C}$ were assessed with the C-HCR system, Figure S7. The fluorescence intensities upon analyzing the two-base and three-base mismatched analytes $\mathbf{I_B}$ (curve c) and $\mathbf{I_C}$ (curve d) are almost the same as the background signal (curve e) of the circuit. Moreover, a distinct signal discrimination was observed between initiator **I** (curve a) and the single-base mismatched analyte $\mathbf{I_A}$ (curve b), demonstrating the high selectivity of the present C-HCR-amplified sensing platform.

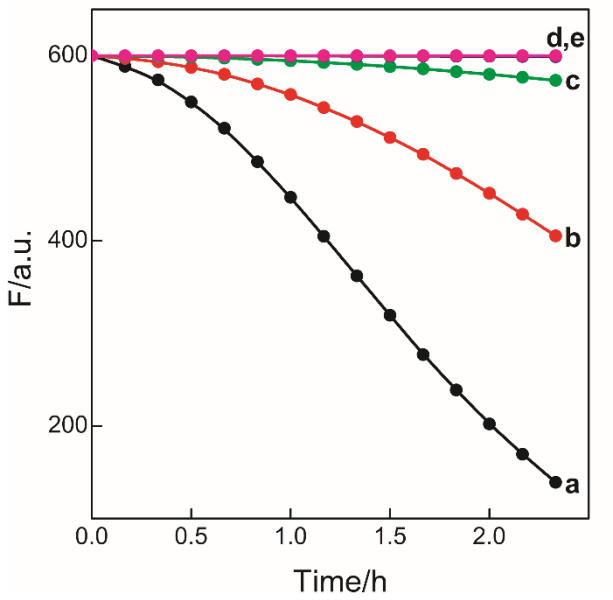

Figure S7. Time-dependent fluorescence changes (at λ=520 nm) upon analysis of different analytes according to Figure 1: (a) **I**, 10 nM, (b) $\mathbf{I_A}$, 10 nM, (c) $\mathbf{I_B}$, 10 nM, (d) $\mathbf{I_C}$, 10 nM, (e) no analyte. The system consisting of $\mathbf{H_1}$+$\mathbf{H_2}$+$\mathbf{H_3}$+$\mathbf{H_4}$+$\mathbf{H_5}$+$\mathbf{H_6}$ mixture (200 nM each) was carried out in reaction buffer (10 mM HEPES, 1 M NaCl, 50 mM $MgCl_2$, pH 7.2).

AFM characterization of the C-HCR-motivated dsDNA branched nanowires

Initiator-activated HCR-1 leads to the formation of tandem catenated triggers for downstream HCR-2 circuit. The upstream HCR-1-generated dsDNA nanowires acted as the backbone that motivated HCR-2 circuit and produced lots of downstream HCR-2 nanowires, resulting in the construction of frond-like branched dsDNA nanostructures. Figure S8 shows AFM images of the C-HCR-motivated dsDNA nanostructure with lower (**A**) and higher (**B**) magnifications. Massive branched dsDNA copolymeric nanowires can be observed from the AFM images.

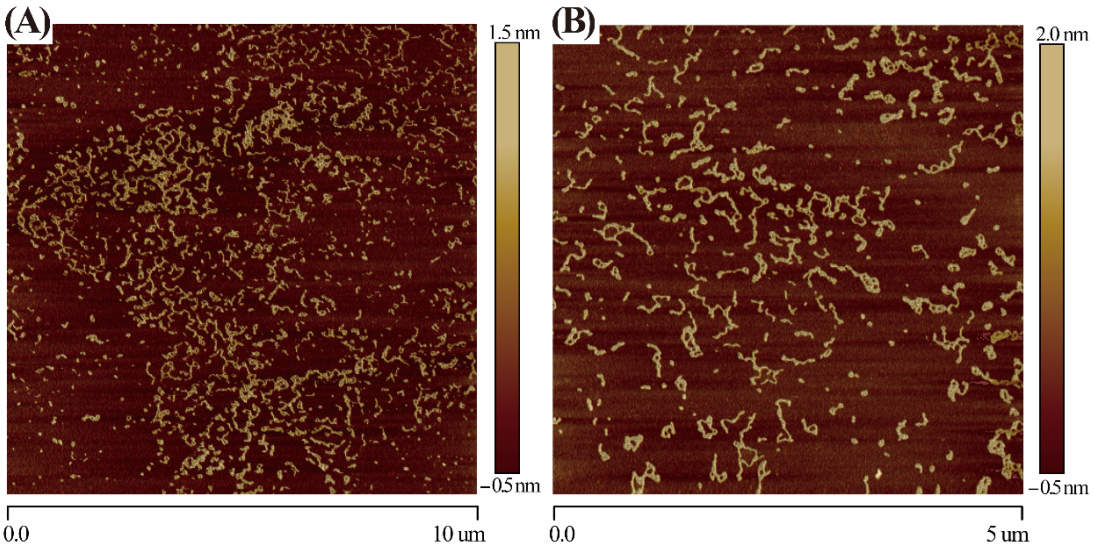

Figure S8. AFM characterization of the C-HCR-motivated dsDNA branched nanowires with lower (**A**) and higher (**B**) magnifications. The mixture consisting of $\mathbf{H_1}$+$\mathbf{H_2}$+$\mathbf{H_3}$+$\mathbf{H_4}$+$\mathbf{H_5}$+$\mathbf{H_6}$ (200 nM each) and initiator **I** (20 nM) was carried out in reaction buffer (10 mM HEPES, 1 M NaCl, 50 mM $MgCl_2$, pH 7.2) for a fixed time interval of 2 h.

The sensitivity and selectivity of the miR-21 sensing platform

The C-HCR amplifier also can be utilized to detect miR-21 by introducing a "helper" hairpin $\mathbf{H_7}$. The hairpin $\mathbf{H_7}$ recognized and hybridized with miR-21. The opened $\mathbf{H_7}$ motivated the sequential cross-hybridizing of C-HCR hairpins mixture, resulting in the assembly of highly branched dsDNA nanostructures. The time-dependent fluorescence changes upon analyzing different concentrations of miR-21 were shown in Figure S9(A). The fluorescence intensity decreased rapidly with increasing concentration of miR-21, originating from the increased formation of HCR-1- and HCR-2-involved nanowires and the efficient generation of FRET signals. Besides the high sensitivity of the C-HCR system, its selectivity was also investigated. Figure S9(B) depicts the time-dependent fluorescence changes upon analyzing 10 nM miR-21 and its control nucleic acids: *β*-actin mRNA, son DNA and let-7a miRNA. Obviously, the fluorescence intensities generated by the different interfering nucleic acids (curve b, c and d, respectively) are almost the same with the background signal (curve a) of the C-HCR system (in the absence of analyte). A significantly decreased fluorescence was observed upon analyzing 10 nM miR-21 (curve e). This clearly demonstrated that the present C-HCR sensing platform has high selectivity and may discriminate the target miRNA from biological interference sequences.

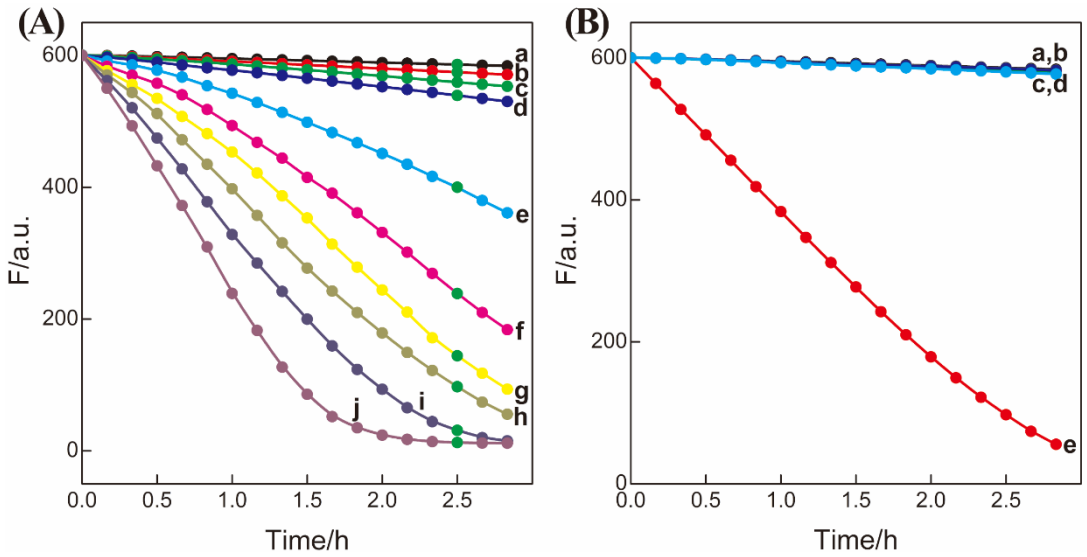

Figure S9. (**A**) Time-dependent fluorescence changes (at λ=520 nm) upon analyzing different concentrations of the target miR-21 using the updated C-HCR sensing platform shown in Figure 4: (a) 0 M, (b) 1×10^{-11} M, (c) 5×10^{-11} M, (d) 1×10^{-10} M, (e) 5×10^{-10} M, (f) 1×10^{-9} M, (g) 5×10^{-9} M, (h) 1×10^{-8} M, (i) 5×10^{-8} M, and (j) 1×10^{-7} M. (**B**) Time-dependent fluorescence changes (at λ=520 nm) upon analysis of different analytes according to Figure 4: (a) no analyte, (b) β-actin mRNA, 10 nM, (c) let-7a, 10 nM, (d) son DNA, 10 nM, and (e) miR-21, 10 nM. The system consisting of $\mathbf{H_1+H_2+H_3+H_4+H_5+H_6}$ mixture (200 nM each) and a "helper" hairpin $\mathbf{H_7}$ (50 nM) was carried out in reaction buffer (10 mM HEPES, 1 M NaCl, 50 mM $MgCl_2$, pH 7.2).

C-HCR-amplified fluorescence imaging of miR-21 in different cells

As shown in Figure S10, the C-HCR system was utilized to detect miR-21 in different living cancer cells. To avoid undesired interfere from the complex cellular environment, we use the fluorescence emission ratio of acceptor to donor (F_A/F_D) as the detecting FRET signal to discriminate microRNA of different expression levels in living cancer cells. An obvious FRET signals were observed for live MCF-7 cells (sample a), indicating a high miR-21 expression level in MCF-7 cells. A comparably decreased FRET signals were observed in live HeLa cell (sample d), indicating the presence of low miR-21 expression in HeLa cell. These results showed that the C-HCR system could distinguish different cell lines with different miRNA expression levels. A slightly weak FRET signals were observed in live MCF-7 cells by conventional HCR system (sample b, $\mathbf{H_6}$-excluded C-HCR imaging strategy), indicating the present C-HCR imaging platform has a comparably enhanced amplification efficacy in living cells as compared to the conventional HCR imaging system. Almost no FRET signals were observed when the miR-21 expression was knocked down by introducing an anti-miRNA antisense inhibitor oligonucleotide into MCF-7 cells (sample c), indicating that the C-HCR system can detect the changes in microRNA expression levels in living cancer cells.

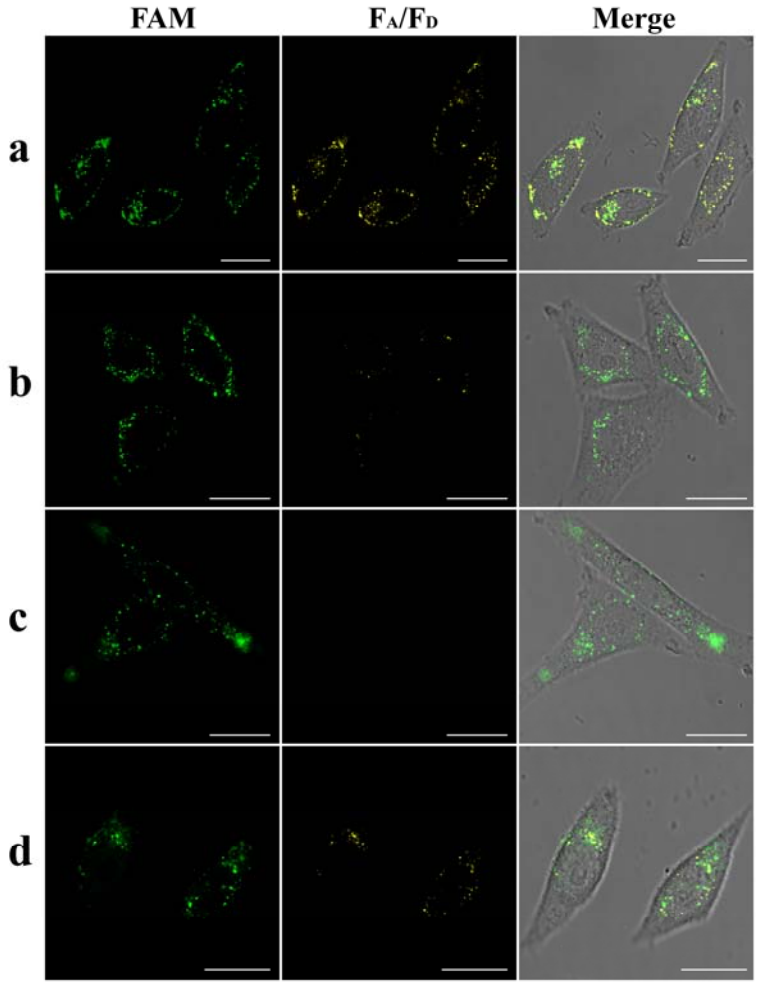

Figure S10. Living cell analysis of miR-21 based on C-HCR or HCR strategy and FRET transduction (in the form of F_A/F_D). Confocal laser scanning microscopy (CLSM) imaging of miR-21 in (a) routine MCF-7 live cells by C-HCR amplifier, (b) routine MCF-7 live cells by conventional HCR amplifier (**H_6**-excluded C-HCR), (c) MCF-7 live cells treated with a chemically modified miR-21 inhibitor by C-HCR amplifier, and (d) HeLa live cells by C-HCR amplifier. All of the aforementioned living cells were transfected and incubated with miR-21-targeting C-HCR or conventional HCR mixture at 37 °C for 2 h. All scale bars correspond to 20 μm.

Control fluorescence imaging experiments of the C-HCR-imaging system

To reveal the high amplified efficiency of the present C-HCR-imaging system, various control experiments were carried out by expelling one of the non-fluorophore-labelled hairpin probes from the C-HCR imaging system, and the results were shown in Figure S11. A high FRET signal was observed in live MCF-7 cells by C-HCR imaging system (sample a), no significant FRET signal was observed for $\mathbf{H_1}$-, $\mathbf{H_2}$- or $\mathbf{H_4}$-excluded C-HCR system (sample c, d and e, respectively) while a slightly weak FRET signal was observed for conventional HCR imaging system (sample b, $\mathbf{H_6}$-excluded C-HCR imaging strategy), indicating the amplification efficacy of the C-HCR imaging platform is indeed enhanced over that of the conventional HCR imaging system in living cells.

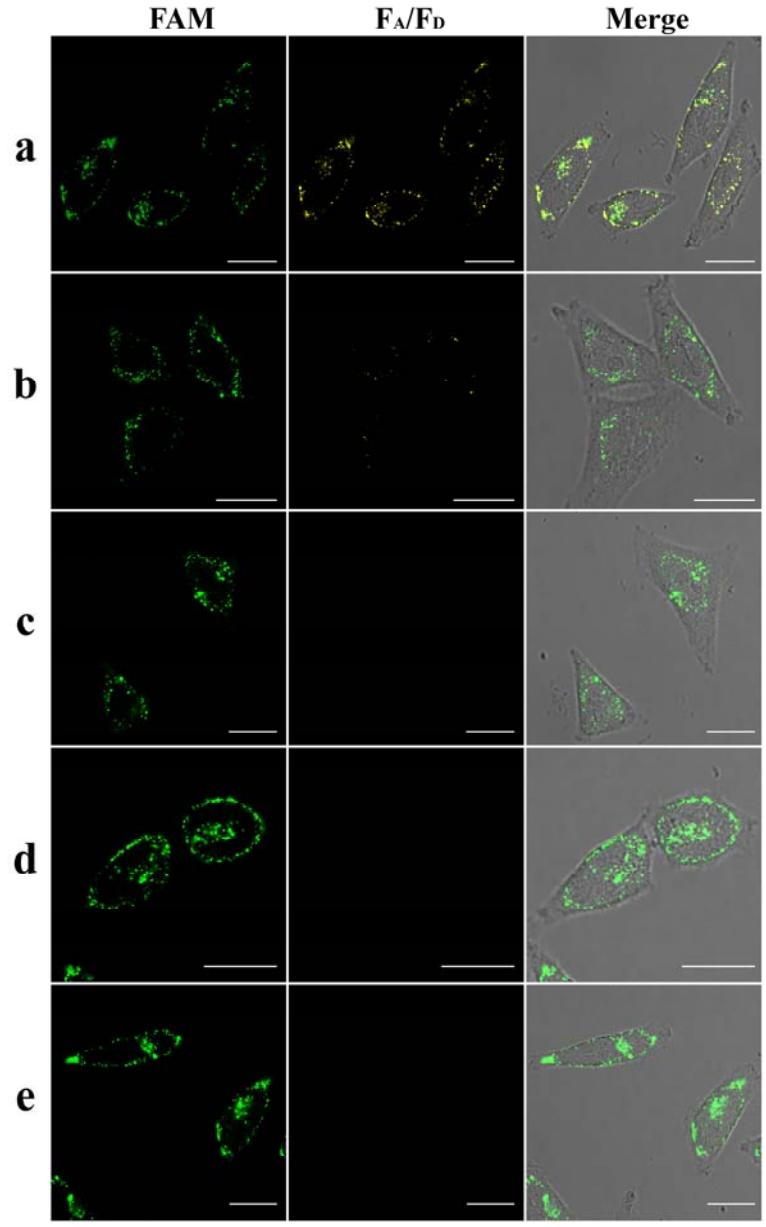

Figure S11. Living cell analysis of miR-21 based on C-HCR-mediated FRET transduction (in the form of F_A/F_D). Confocal laser scanning microscopy (CLSM) imaging of miR-21 in routine MCF-7 live cells that were respectively transfected and incubated with the original C-HCR system (a), the **H**$_6$-excluded C-HCR system (b), the **H**$_1$-excluded C-HCR system (c), the **H**$_2$-excluded C-HCR system (d), and the **H**$_4$-excluded C-HCR system (e) at 37 °C for 2 h. All scale bars correspond to 20 μm.

FRET efficiency of the CHCR-imaging system

The FRET efficiency of fluorescence imaging systems was acquired by a conventional acceptor-photo-bleaching technique (Figure S12). Here, the acceptor (TAMRA)-photo-bleaching-induced fluorescent intensity changes of the donor (FAM) were analyzed and calculated for obtaining reliable FRET efficiency of the C-HCR imaging system. The fluorescence of FAM donor could be restored after photobleaching TAMRA acceptor. The luminescence intensities of FAM donor were recorded before and after the photobleaching of TAMRA acceptor, and provided a direct way for quantifying the FRET efficiency ($FRET_{eff}$) as follows:

$$FRET_{eff} = (D_{post} - D_{pre})/D_{post}$$

where D_{pre} and D_{post} correspond to the fluorescence intensities of FAM donor before and after TAMRA-photobleaching, respectively.

For reliability and accuracy purposes, the FRET efficiency was derived from different regions and sets of the living cells. And the calculated average FRET efficiency corresponds to 0.62 (Figure 6(C)).

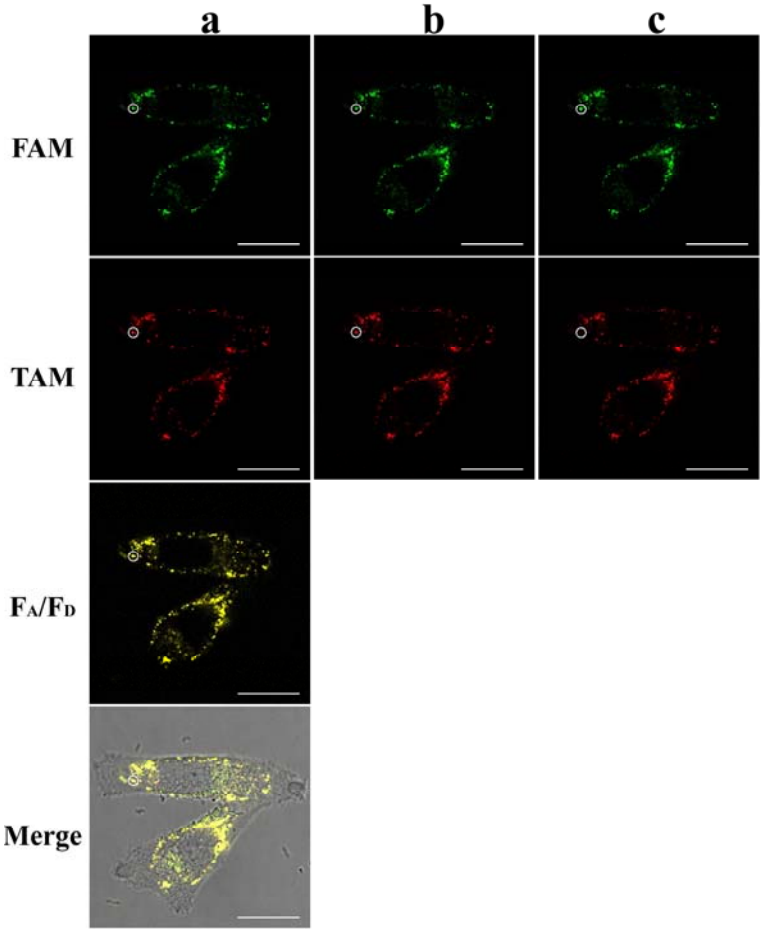

Figure S12. Estimation of the FRET efficiency of the present C-HCR-imaging system through confocal laser scanning microscopy (CLSM) imaging of routine MCF-7 live cells (a). A selected region of MCF-7 cells was used as an example to show how to acquire the FRET efficiency of C-HCR-imaging system by photobleaching the TAMRA acceptor of FAM/TAMRA (donor/acceptor) FRET pair. CLSM imaging of miR-21 in routine MCF-7 living cells before (b) and after (c) photobleaching of TAMRA acceptor. All scale bars correspond to 20 μm. All routine MCF-7 living cells were transfected and incubated with miR-21-targeting C-HCR mixture at 37 °C for 2 h.

Table S3. Comparison of different fluorescence methods for nucleic acid detection.

System	Sensing duration(h)	Sensitivity (M)	Ref.
Carbolic regeneration of analyte by DNAzyme amplification	12	1×10^{-12}	[1]
Catalytic hairpin assembly-mediated mRNA imaging in cells	2	5×10^{-10}	[2]
Amplified Analysis of DNA based on HCR-DNAzyme cascade	12	1×10^{-14}	[3]
HCR-mediated detachment of DNA probe from graphene oxide	4.5	1×10^{-12}	[4]
HCR-mediated detachment of DNA probe from gold nanoparticles	3	5×10^{-13}	[5]
HCR-mediated in situ visualization of tumor-related mRNA	4	1.8×10^{-11}	[6]
Graphene oxide-assisted HCR-mediated two-color imaging of miRNA	8	1.8×10^{-13}	[7]
C-HCR-mediated nucleic acid detection and miRNA imaging	2	3×10^{-12}	This work

References

[1] F. Wang, J. Elbaz, C. Teller and I. Willner, *Angew. Chem., Int. Ed.*, 2011, **50**, 295-299.

[2] C. C. Wu, S. Cansiz, L. Q. Zhang, I. T. Teng, L. P. Qiu, J. Li, Y. Liu, C. Zhou, R. Hu, T. Zhang, C. Cui, L. Cui and W. H. Tan, *J. Am. Chem. Soc.*, 2015, **137**, 4900-4903.

[3] F. Wang, J. Elbaz, R. Orbach, N. Magen and I. Willner, *J. Am. Chem. Soc.*, 2011, **133**, 17149-17151.

[4] L. Yang, C. Liu, W. Ren and Z. Li, *ACS Appl. Mater. Interfaces*, 2012, **4**, 6450-6453.

[5] Z. Wu, G. Q. Liu, X. L. Yang and J. H. Jiang, *J. Am. Chem. Soc.*, 2015, **137**, 6829-6836.

[6] J. Huang, H. Wang, X. Yang, K. Quan, Y. Yang, L. Ying, N. Xie, M. Ou and K. Wang, *Chem. Sci.*, 2016, **7**, 3829-3835.

[7] L. Li, J. Feng, H. Liu, Q. Li, L. Tong and B. Tang, *Chem. Sci.*, 2016, **7**, 1940-1945.